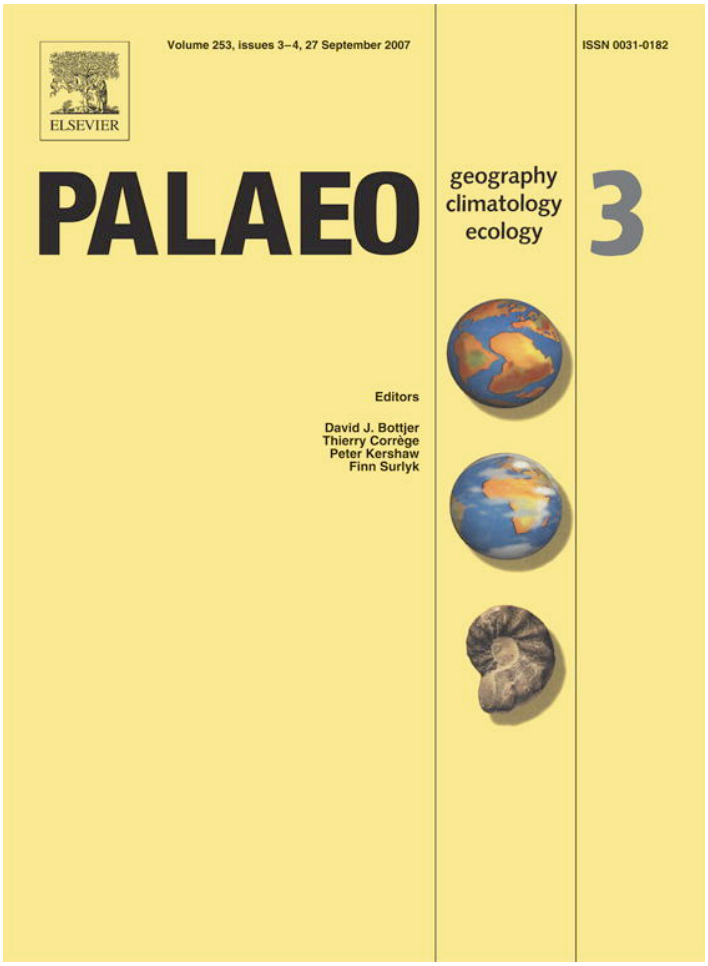

Available online at www.sciencedirect.com
ScienceDirect
ELSEVIER
PALAEO
Palaeogeography, Palaeoclimatology, Palaeoecology 253 (2007) 509–528
www.elsevier.com/locate/palaeo

A numerical study of the South Atlantic circulation at the Last Glacial Maximum

Gabriel Clauzet [a,*], Ilana Wainer [b], Alban Lazar [c], Esther Brady [d], Bette Otto-Bliesner [d]

[a] *ASA South America, Rua Purpurina 155, Cj 96, 05435-030, São Paulo, Brazil*
[b] *Department of Physical Oceanography, University of Sao Paulo, Brazil*
[c] *LODYC-IPSL, Université Pierre et Marie Curie, Paris, France*
[d] *National Center for Atmospheric Research, Boulder, Colorado, USA*

Received 4 December 2006; received in revised form 11 June 2007; accepted 19 June 2007

Abstract

In this study, we examine the simulation results from the paleoclimate version of the National Center of Atmospheric Research coupled Climate System Model (CSM 1.4) for the Last Glacial Maximum (LGM) in order to understand changes in the South Atlantic (SA) circulation relative to the Present Day (PD). The LGM simulation is validated with the available proxy data in the region. The results show good agreement, except in the eastern equatorial and eastern SA region, where the model is not able to reproduce the correct cloud cover and the associated air–sea interactions. Ocean transport in the PD simulation is in good agreement with observational estimates. Results show that at subsurface levels there are two distinct patterns: (i) strengthening of the transport for the LGM in the southern SA (35°S to 25°S); and (ii) weakening of the mass transport in the northern SA (25°S to the Equator). In intermediate layers, there is an intensification of the subtropical gyre and a northward shift of the South Equatorial Current (SEC) bifurcation for the LGM. This leads to the intensification of the southward transport by the Brazil Current (BC) and the associated BC recirculation cell in the southern basin for the LGM. This shift in the position of the SEC bifurcation leads to a weakening in the northward transport and the western recirculation of the central SEC in the northern basin. This northward shift of the SEC (upper limit of the subtropical gyre) is consistent with the northward shift observed in the subtropical convergence zone and suggests a displacement of the sub-tropical gyre 3°–5° towards the Equator. In deeper layers, a shallower and weaker North Atlantic Deep Water (NADW) circulation in the LGM contributes to the reduction of the southward transport in the northern part of the basin and is associated with a greater northward intrusion of Antarctic Bottom Water. This intrusion plus the increase of the Indian Water inflow is responsible for the northward transport intensification in the southern basin.

Keywords: Coupled climate model; Last Glacial Maximum; Ocean circulation; South Atlantic; Paleoceanography; Paleoclimatology

1. Introduction/Background

The study of past climates plays an essential role in understanding the natural variability of the climate system and modeling of past climates tests model sensitivity for extreme climates. The redistribution of mass and heat by the atmosphere and ocean is one of the most important aspects of the climate system, given that variations in oceanic heat and mass transport have been suggested as causes of abrupt climatic change. The pathways and mechanisms of oceanic transport in the past are critical issues in understanding the present climate state and the

* Corresponding author. Tel.: +55 11 34443740; fax: +55 11 34443748.
E-mail address: gclauzet@usp.br (G. Clauzet).

0031-0182/$ - see front matter © 2007 Elsevier B.V. All rights reserved.
doi:10.1016/j.palaeo.2007.06.018

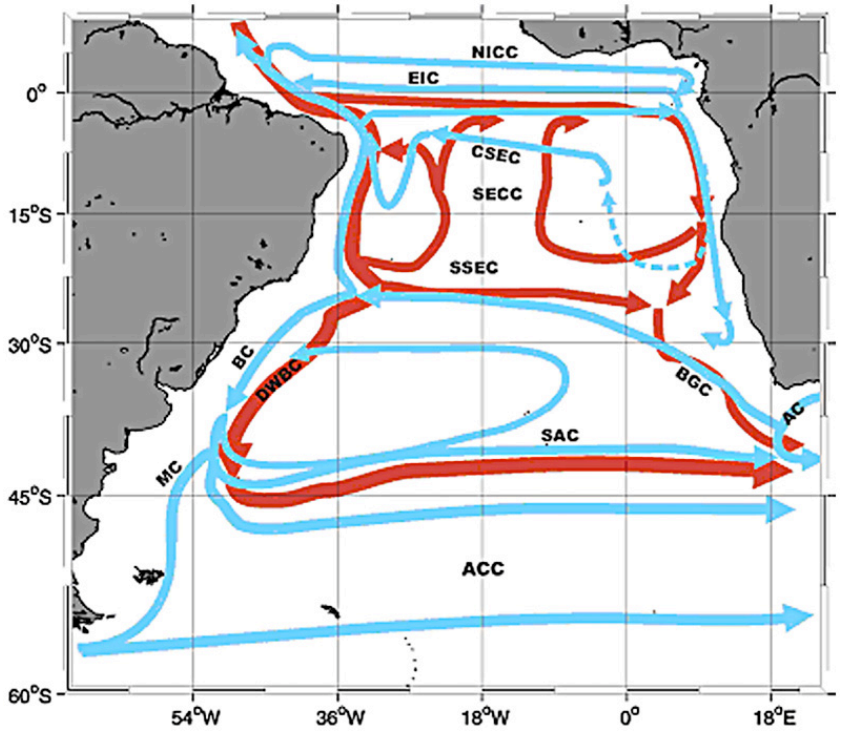

Fig. 1. Schematic representation of the large-scale South Atlantic circulation. In blue, the intermediate geostrophic currents (about 500 to 1200 m). In red, the deep flow (near 2000 m depth). Shown are the Malvinas Current (MC); the Brazil Current (BC); the South Atlantic Current (SAC); the Benguela Current (BGC); the Antarctic Circumpolar Current (ACC); the South Equatorial Current (SEC); with the southern (SSEC) and central (CSEC) branches; the South Equatorial Countercurrent (SECC); Equatorial Intermediate Current (EIC); Northern Intermediate Countercurrent (NICC) (adapted from Stramma and England, 1999). (For interpretation of the references to colour in this figure legend, the reader is referred to the web version of this article.)

possibilities of future changes. In this context, the South Atlantic is a unifying link for exchanging waters of the world's major ocean basins and is the only ocean basin in the Southern Hemisphere that transports heat equatorward (Gordon, 1986).

The dominant horizontal circulation in the South Atlantic is the anticyclonic Subtropical Gyre. Four major currents delimit the Subtropical Gyre (see Fig. 1): to the east the Benguela Current (BGC), to the north the South Equatorial Current (SEC), the Brazil Current (BC) delimits the western boundary, and at the southern edge the South Atlantic Current (SAC). Three other currents are also important for the circulation associated with the Subtropical Gyre: the Malvinas Current (MC), the Agulhas Current (AC), and the Antarctic Circumpolar Current (ACC).

The BGC begins as a northward flow off the Cape of Good Hope, and flows along the African coast before it splits into two branches near 30°S (Peterson and Stramma, 1991). The first branch continues to flow northward parallel to the coast; the second branch flows northwest into the SEC. The water of the BGC is replenished from two routes. The warm route (Gordon, 1986) originates in the AC and supplies the BGC with large eddies shed from the Agulhas Retroflection, which transports warm water from the Indian Ocean. The second one, called the cold route (Rintoul, 1991), comes from the SAC and contains the relatively cold water from the South Atlantic Central Water and Antarctic Intermediate Water (Pickard and Emery, 1982). This branch of the subtropical gyre is responsible for the northward transport of surface and thermocline waters. Estimates of the magnitude of the associated flows are important to understanding of the South Atlantic.

Several studies estimate the transports of the BGC and AC. These observational estimates provide an excellent opportunity to evaluate how well the numerical model used here simulates the ocean dynamics in the present. For the BGC transport, Sverdrup et al. (1942) was the first to estimate the value of 18.7 Sv at 30°S relative to 1200 m; Fu (1981) calculated the geostrophic transport at 500 m across 32°S to be 20 Sv and Stramma and Peterson (1989) found it to be 21 Sv at 32°S and 18 Sv at 30°S, away from the coast. These results indicate that the average Benguela transport across 30°S is about 20–25 Sv.

The AC is a western boundary current in the South Indian Ocean. It flows down the east coast of Africa

from 27°S to 40°S (Gordon, 1985). The AC reaches the southern tip of Africa and begins to turn toward the southwest. Once it reaches the Southern Ocean, the current retroflects and flows eastward as the Agulhas Return Current (Quartly and Srokosz, 1993). The AC system transports large volumes of water. Gordon (1985) found a transport of 67 Sv. Beal and Bryden (1999) found a geostrophic volume transport of 73 Sv. In a later work, Bryden and Beal (2001) found a net transport about 70 Sv in the region.

Originating from the BGC in the eastern South Atlantic, the SEC marks the northern limit of the Subtropical Gyre. It flows westward across the Atlantic between 25°S and 10°S. Near the Brazilian coast, at Cabo de São Roque, the SEC bifurcates with one branch, the stronger of the two, heading northwards as the North Brazil Current (NBC) and the other flows southward as the BC. The BC is the western limit of the Subtropical Gyre. This western boundary current flows along the continental shelf transporting warm and salty waters southward. Gordon and Greengrove (1986) estimate that the BC increases at a rate of 5% per 100 km south of 24°S. Stramma (1989) estimated the BC transport at 23°S to be about 10 Sv and at 33°S to be about 17.5 Sv. This 7.5 Sv increase was accounted for by a recirculation cell of roughly the same magnitude beginning at about 28°S. Between approximately 40°–35°S the BC encounters the MC. The MC is a branch of the AAC and flows northward along the continental shelf of Argentina until it reaches the BC offshore the Rio de la Plata estuary (Legeckis and Gordon, 1982; Garzoli, 1993). In the region known as the Brazil–Malvinas Confluence (BMC), this strong, relatively fresh, and cold flow meets the weak, warm, southward-flowing Brazil Current. In this energetic region a sharp gradient in temperature and salinity is observed (Wainer et al., 2000; Goni and Wainer, 2001).

The southern limit of the subtropical gyre is the SAC. The SAC is separated from the ACC by the Subtropical Front (SF) (Stramma and Peterson, 1990). The eastward flowing SAC feeds the BGC, the AC and the South Indian Current (SIC). The ACC is the most important current in the Southern Ocean, and the only current that flows completely around the globe. The ACC flows eastward into the South Atlantic through the Drake Passage and leaves between Cape of Good Hope and the Antarctic Peninsula entering the Indian Ocean. Large ranges of transport values for the ACC have been found by numerous oceanographers at the Drake Passage. Pickard and Emery (1982) estimate a transport of 139 Sv for the ACC. Whitworth and Peterson (1985) estimate a similar transport, around 123 Sv for the same region. In recent years, other areas such as sections of the ACC south of Tasmania and New Zealand have revealed a mean ACC transport of 100–150 Sv (Knauss, 1996).

Since the North Atlantic basin is practically closed to the north, the South Atlantic acts as a link to other oceans, exporting deep dense waters, which are formed in the high latitude, and receiving shallow warm waters closing the thermohaline cell. The warm water path enters the South Atlantic via the Agulhas leakage, and flows to the north through the BGC, SEC, NBC and Gulf Stream. The cold water path leaves the Atlantic by the Deep Western Boundary Current (DWBC) and returns through the Drake Passage through the ACC. Changes in these pathways have been suggested to be the causes of climatic changes during the Last Glacial Maximum (Broecker and Denton, 1990; Broecker, 1997).

In this work, we compare the main differences in the South Atlantic circulation pathways and mass transport between the LGM and the Present Day (PD) climates as simulated by a fully coupled numerical model. Considering that the South Atlantic plays an important role in the global circulation, a better understanding of its dynamics can improve our knowledge about glacial climate changes.

2. The numerical model

We have used a version of the National Center for Atmospheric Research–Community Climate System Model (NCAR–CCSM) that is designed for long-term climate simulations (Otto-Bliesner and Brady, 2001). The numerical coupled model is composed of four components: atmospheric, oceanic, land surface and sea-ice (Boville and Gent, 1998). The atmospheric component of this model is the Community Climate Model (CCM), version 3.6, with T31 resolution (approximately 3.75° in latitude and longitude) and 18 vertical levels (Kiehl et al., 1998; Hack et al., 1998). The ocean component (NCOM) of this model was developed from the Geophysical Fluid Dynamics Laboratory z-coordinate primitive equation model (Gent et al., 1998). The spatial resolution is 3.6° in longitude, with variable resolution in latitude ranging from 1.2° at the tropics to 2.3° at the poles, and 25 vertical levels. The sea-ice model (CSIM) dynamics is based on the cavitating fluid rheology (Flato and Hibler, 1992; Weatherly et al., 1998). The land-surface model provides a comprehensive treatment of land surface processes allowing for different vegetation types (Bonan, 1998).

The major difference between the LGM and the present-day simulations are the change of the earth's orbital parameters, the presence of ice sheets, the reduction of atmospheric greenhouse gases and the increase of the atmospheric dust load. Combinations of

the model components (atmospheric, sea-ice, ocean and land) are integrated separately to obtain an appropriate initial state of the coupled system prior to full coupling. The ocean and the sea-ice models are spun-up for 20 (Modern ocean) and 40 (LGM ocean) surface model years, which is the equivalent to 1000 and 2000 model years using the deep acceleration technique (Bryan, 1984). The coupled control simulation (referred as Present Day (PD) simulation) is performed for 110 years using pre-industrial levels of greenhouse gases (280 ppmv for CO_2, 0.8 ppmv for CH_4, 0.288 ppmv for N_2O, and no chlorofluorocarbons). The coupled LGM integration is performed for the same period, starting from an initial condition that is produced using the Climate/Long Range Investigation Mappings and Predictions Project (CLIMAP, 1981) sea surface temperature (SST). The LGM simulation uses CO_2 concentrations of 200 ppmv. Concentrations of other atmospheric greenhouse gases follows Raynaud et al. (1993), ice sheets are prescribed as in Peltier (1994) and the orbital parameters of 21 kyr ago (Berger, 1978) are used to determine the total solar flux. In both runs, the last 50 years was used to calculate the mean climatology. More details about the LGM simulation are described in Shin et al. (2003b).

3. Results

3.1. Validation of intermediate and deep circulation for the present-day

To validate the model circulation, we compare the results for the PD with the schematic representation of the large-scale circulation of the South Atlantic made by Stramma and England (1999), based on hydrographic data and model simulations. Fig. 1 depicts the depth averaged simulated streamlines for intermediate (about 500 to 1200 m) and the deep ocean circulation (near 2000 m) (blue and red lines, respectively). The streamlines representing the pathways of the total mean flow are shown in Fig. 2 (using the previous color scheme). In most respects, the simulated circulation (Fig. 2) compares well to the schematic circulation shown in Fig. 1. At the southern part of the SA, the intermediate circulation shows a strong ACC and its northward flowing branch, representing the MC. To the north, the Brazil–Malvinas Confluence region and the currents that are part of the subtropical gyre are well represented.

In the equatorial region, the large scale circulation is simulated poorly. Lack of sufficient model resolution near the Equator may prevent accurate simulation of the complex dynamics in the equatorial region. However, even a higher-resolution CSM ocean component, forced stand-alone by observed SST, produces a poor simulation of the tropical Atlantic. Near the African coast, the model shows some characteristics of the southern branch of the South Equatorial Current (SSEC), the return current South Equatorial Countercurrent (SECC) at 10°S, and the central branch of the South Equatorial Current (CSEC) at 5°S. However, the model is unable to represent the Agulhas retroflection. In fact, caution should be taken in the interpretation of the results related to the Agulhas region. The Agulhas Current, its retroflection, and mesoscale and submesoscale features are underestimated if not completely absents in the

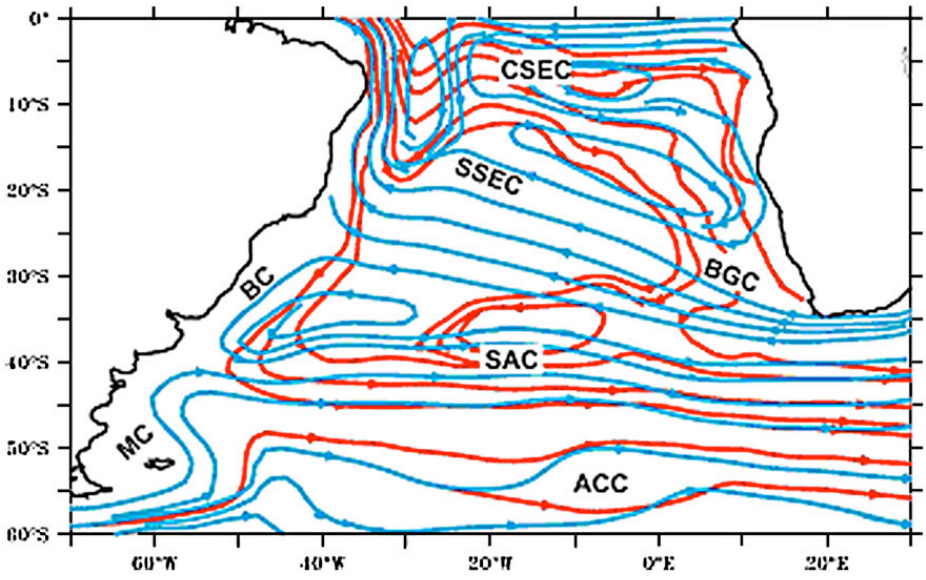

Fig. 2. Streamlines at intermediate depth (averaged from 500 to 1200 m) in blue and at deep layer (2000 m) in red. Current names are as in Fig. 1. (For interpretation of the references to colour in this figure legend, the reader is referred to the web version of this article.)

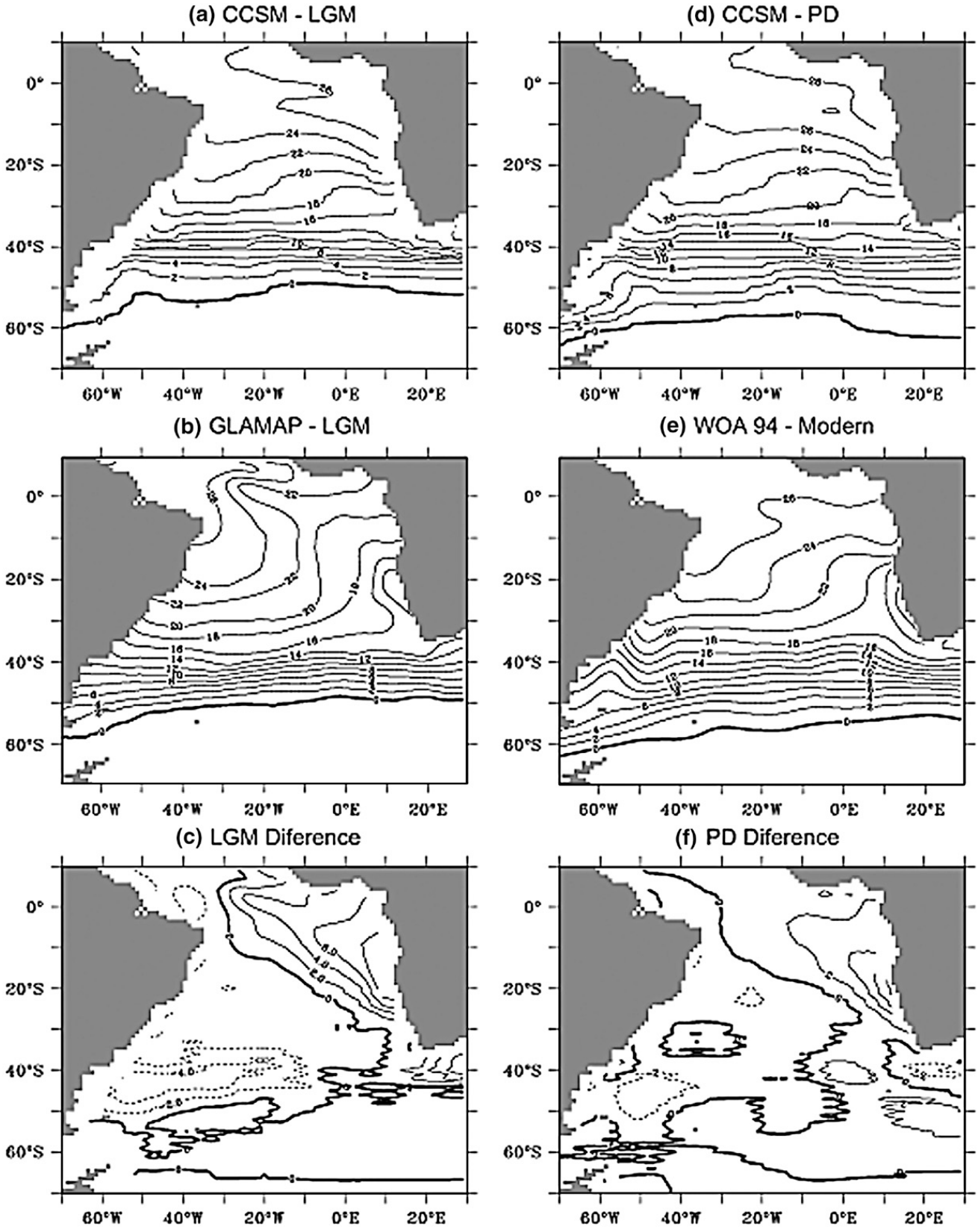

Fig. 3. Annual mean SST for the Equatorial and South Atlantic: (a) CCSM LGM simulation; (b) GLAMAP reconstruct LGM; (c) anomaly map (CCSM LGM minus GLAMAP); (d) CCSM present-day (PD) simulation; (e) modern; (f) anomaly map (CCSM PD minus modern). Modern SSTs are atlas data, derived from 1° × 1° grid (Levitus and Boyer, 1994).

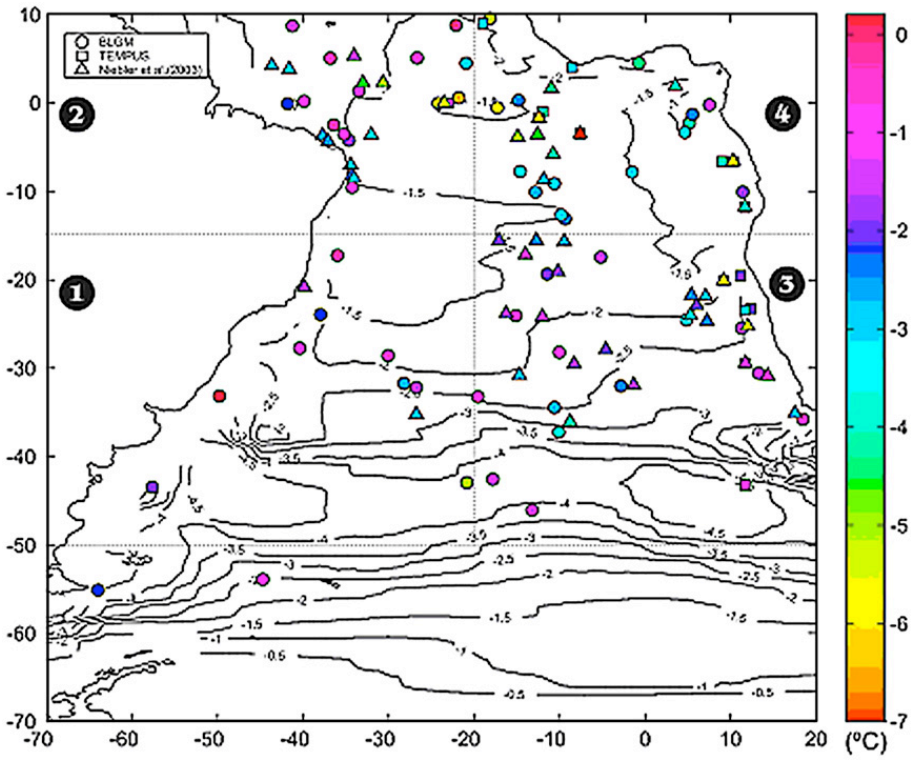

Fig. 4. Sea surface temperature anomaly (LGM minus modern) (°C). Database: Circles: BLGM (Trend-Staid and Prell, 2002); Squares: TEMPUS (Rosell-Melé (1998); Triangles: Niebler et al. (2003). The contours represent the CCSM anomaly (LGM minus PD simulation). The thin dashed line delimits the four boxes described in the text: western and eastern South (boxes 1 and 3, respectively) and Tropical (boxes 2 and 4, respectively).

CCSM. The Angola Gyre, represented by the dashed line in Fig. 1, does not appear at this depth in the model, but can be seen closer to the surface. At the Brazilian coast the North Brazil Undercurrent (NBUC) and the recirculation of the central band of the SEC (CSEC) are well represented.

The deep circulation is dominated by the spreading of the North Atlantic Deep Water (NADW). The DWBC transports the NADW from the Northern Hemisphere into the SA. After crossing the Equator the flow splits in two parts. One still flows to the south following the DWBC; the other part flows eastward across the Atlantic to the African coast. According to Stramma and England (1999), part of the NADW should recirculate in the Brazil Basin and in the Angola Basin. These two recirculations are not evident in the PD simulation.

3.2. Validation of LGM-simulated SST with the available proxy data

The modeling community has largely relied on the reconstruction of the LGM by the CLIMAP Project (1981) to evaluate model performance. In the last two decades, some elements of CLIMAP have been questioned (see a detailed account in Mix et al., 2001; Pflaumann et al., 2003). But only recently has there been a considerable effort to review the CLIMAP data set on a global scale. The EPILOG project (Environmental Processes of the Ice age: Land, Oceans, Glaciers) and its offshoot the MARGO project (Multiproxy Approach for the Reconstruction of the Glacial Ocean Surface) are laying out the strategies to undertake new syntheses of the climate at the LGM (Mix et al., 2001; Clark and Mix, 2002). This effort led to the development of the GLAMAP 2000 (Glacial Atlantic Ocean Mapping) project (Sarnthein et al., 2003; Pflaumann et al., 2003). This new reconstruction of the glacial SST in the Atlantic is based on census counts of planktonic foraminifera, using the Maximum Similarity Technique Version 28 (SIMMAX-28) modern analog technique with 947 modern analog samples and 119 well-dated sediment cores. Paul and Schafer-Neth (2003) used the GLAMAP-reconstructed SST to produce gridded monthly sea surface boundary conditions for the Atlantic Ocean at the LGM. In this section, we evaluate the results of the LGM simulated SST from the NCAR coupled model with the gridded fields produced by Paul and Schafer-Neth (2003). The present-day simulation is evaluated with the World Ocean Atlas (WOA 94) data set (Levitus and Boyer, 1994). Other data proxies based on different analyses (transfer function method with planktonic foraminiferal assemblages, alkenones,

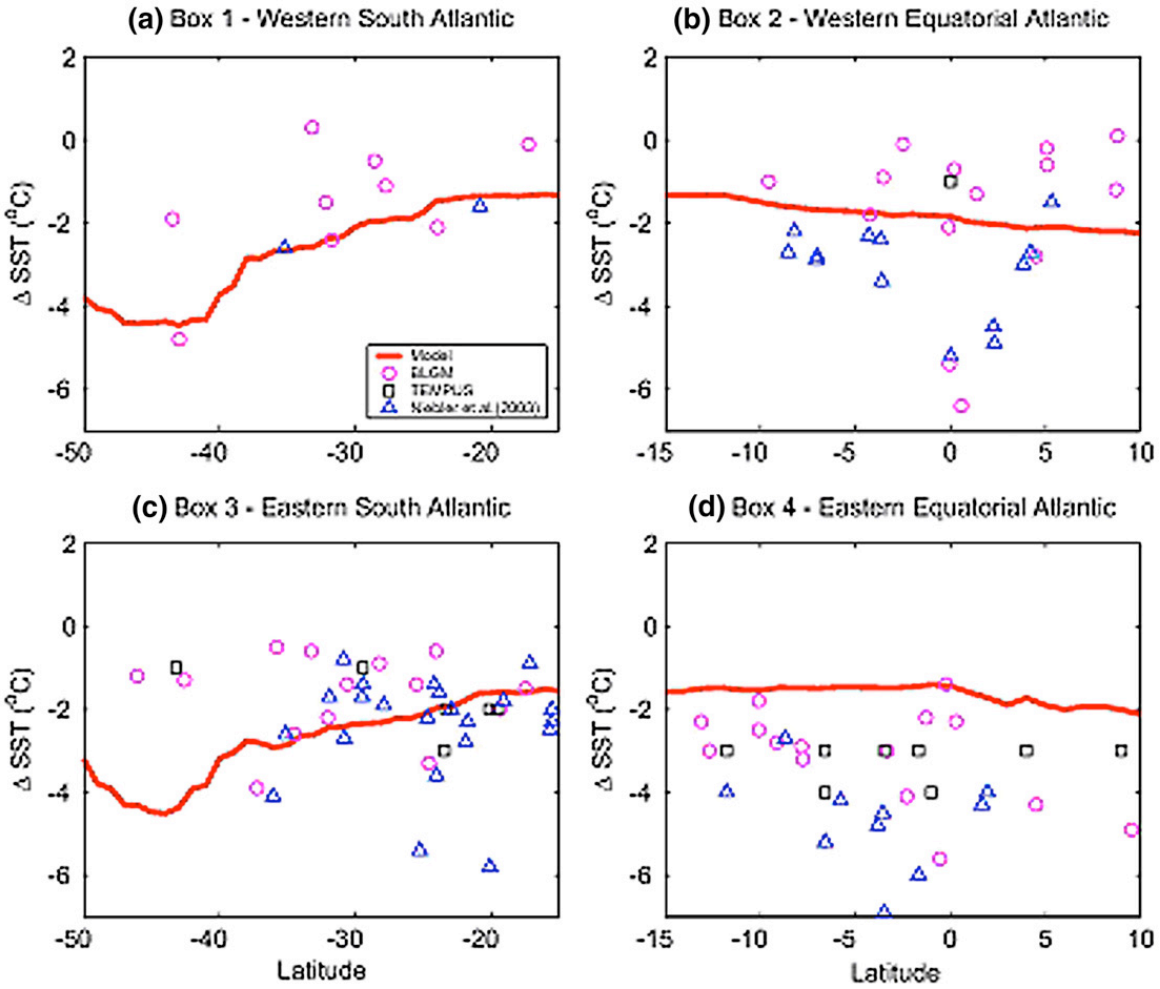

Fig. 5. Zonally averaged sea surface temperature anomaly (LGM minus modern) (°C). The database and markers are described in Fig. 4. Solid line represents the CCSM simulation. Western: (a) Box 1 – South Atlantic, (b) Box 2 – Equatorial Atlantic. Eastern: (c) Box 3 – South Atlantic; (d) Box 4 – Equatorial Atlantic.

dinocyst assemblages) are also compared to the model results. Individual proxy estimates are compared with the area averaged model climate in selected regions (a method successfully used in PMIP simulations (Pinot et al., 1999)).

Fig. 3 shows the annual averaged SST fields for the LGM (a); Present Day simulation (d); GLAMAP (b); WOA 94 (e); and their differences (Fig. 3c and f). In the LGM proxy SST data, the warmest waters are restricted to the western part of the equatorial Atlantic (Fig. 3(b)). In the PD observed SST data, the warmest water penetrates eastward into the Gulf of Guinea (Fig. 3(e)). The PD simulation shows similar temperatures around 26 °C in the equatorial region, but with a warm region in the eastern part of the basin. This shows the known shortcoming of the model in reproducing the upwelling region in the eastern equatorial Atlantic. Substantial cooling is seen in the eastern part of the South Atlantic near the African coast (Fig. 3b) at the LGM when compared to WOA 94 (Fig. 3c). The cool water flows northwest towards the Equator. This intrusion of cold water in the tropical region suggests an intensification of the oceanic branch of the Benguela Current which carries cold Southern Ocean waters northward. The mean position of the Subtropical Convergence Zone (SCZ) in the modern South Atlantic is around 40°S (Fig. 3e) coinciding with SST isotherms of 12 °C to 16 °C. Using these isotherms as a guide to locate the SCZ in the GLAMAP reconstruction we can see a northward shift in the SCZ position around 4°–5° latitude in the west and 15° latitude in the east (Fig. 3b). The LGM simulation results (Fig. 3a) also show a northward shift in the 12–16 °C isotherms by 3° to 8° latitude with the largest shift in the east. Trend-Staid and Prell (2002) found a similar feature in their reconstruction, but with a small shift in the eastern basin. They concluded that this shift in the LGM SCZ is consistent with a compression and/or equatorward shift of the

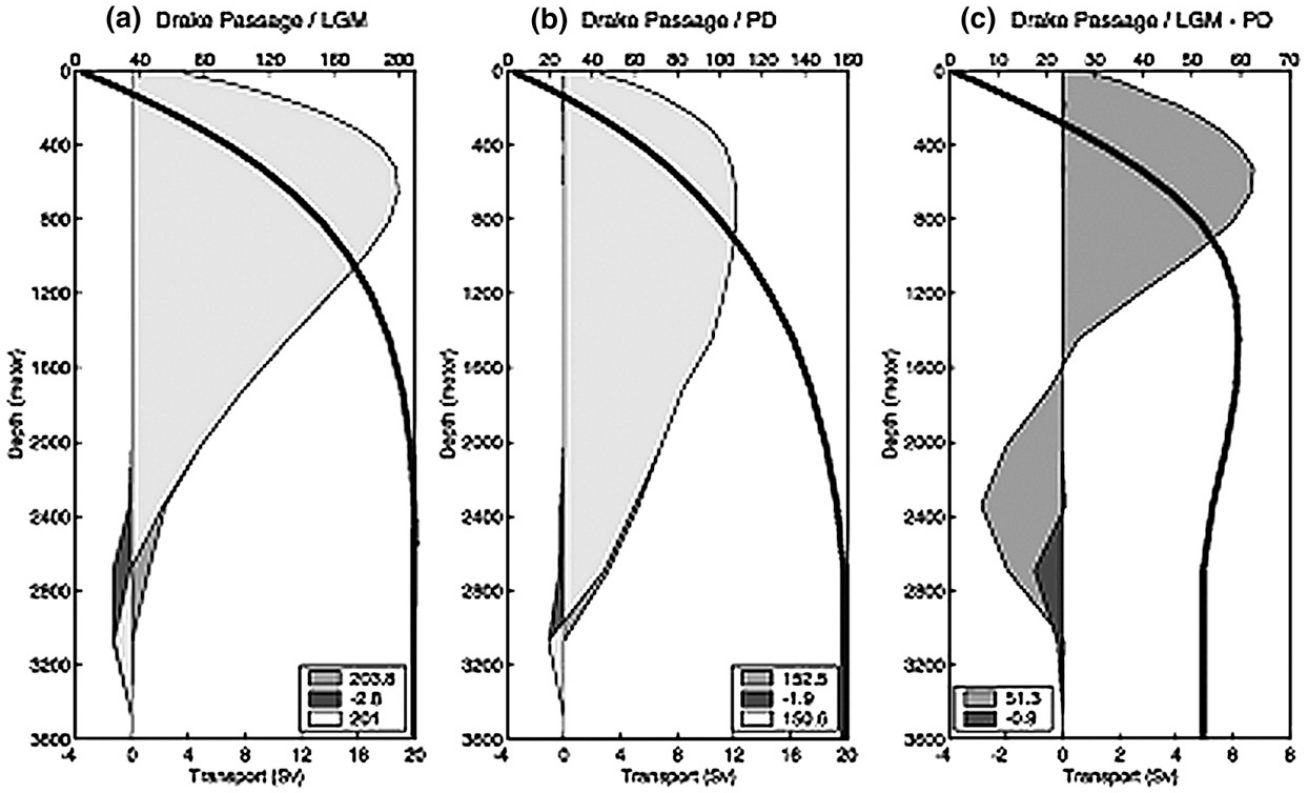

Fig. 6. Volume transport (Sverdrups, 1 Sv = 10^6 m^3 s^{-1}) by depth for the Drake Passage (near 68°W) for the Present Day (PD), LGM and their difference (LGM − PD). Positive fluxes are to the east. In dark gray is the eastward transport, black the westward and light gray the net transport (bottom *x*-axis). The legend shows the total transport for each direction. The thick black line shows the total eastward-integrated transport (top *x*-axis).

subtropical gyre. Near the Brazil–Malvinas Confluence region, the enhancement of the SST gradient for the GLAMAP produces negative differences between 30°S and 50°S (Fig. 3c). Largest differences are found in the eastern SA, with a maximum around 8 °C near the Angola Gyre (Fig. 3c). This huge difference could be attributed to different causes associated with both proxy data uncertainty and numerical model limitations. The GLAMAP data set has some conflicts between the temperatures reconstructed from fossil plankton species and those from geochemical proxy measurements (Mix, 2003). These conflicts produce some sharp differences between the temperature proxies in the eastern equatorial Atlantic (Pflaumann et al., 2003) and the Namibian upwelling system (Niebler et al., 2003).

Large and Danabasoglu (2006) discuss that the atmosphere has been shown to only partially explain the coastal biases, so the ocean may play a significant role. Coastal upwelling is known to bring cool water to the surface. It is driven by the surface Ekman divergence in response to the alongshore component of near-coastal winds. However, the strength and temperature are not known quantitatively, so it is unclear how well it is being represented in any model configuration.

A significant bias exists in the net energy flux into the eastern boundaries of Pacific and Atlantic Oceans associated with a poor simulation of coastal (stratus) clouds in the coupled model. In particular, the cloud fraction of marine stratus is underestimated so that the resulting energy flux bias has serious implications for the CSM simulations. The lack of marine stratus cloud in these regions also produces small downward longwave fluxes, compared to the observations (shown by Kiehl et al., 1998). The marine stratus regions off the western coast of North and South America and off Africa are too warm by 2–3 °C, resulting from the bias in cloud simulation in CCM3 (atmospheric component of the coupled model; Boville and Hurrel, 1998; Norris and Weaver, 2001). This results in a weak east–west pressure gradient at the Equator which in turn translates into weaker zonal winds. The too-weak zonal wind stress along the Equator in the coupled model affects the SST in two ways. First, it leads to a deepening of the thermocline in the eastern part of the basin and a shallowing in the western part. Second, the weak zonal stress leads to a vertical velocity distribution at the based of the mixed layer that is too weak in the eastern and central Atlantic and too strong in the western Atlantic.

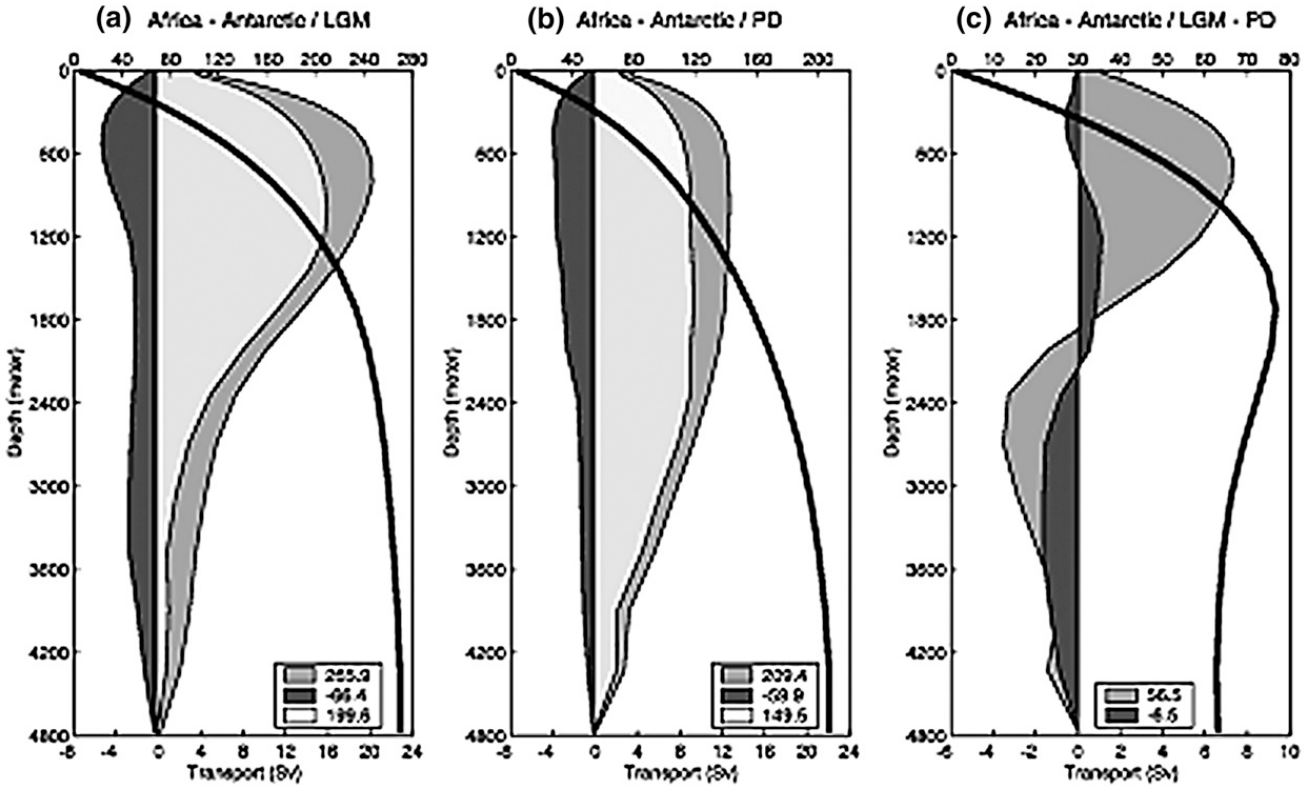

Fig. 7. Volume transport (Sv) by depth along the section between Cape of Good Hope and the Antarctic Peninsula (at 18°E) for the Present Day (PD), LGM and their difference (LGM − PD). Positive fluxes are to the east. In dark gray is the eastward transport; black the westward and light gray the net transport (bottom *x*-axis). The legend shows the total transport for each direction. The thick black line shows the total eastward-integrated transport (top *x*-axis).

Both of these errors lead to insufficient cooling of the eastern near equatorial mixed layer leading to a warming. Furthermore, studies that compares the surface energy budget of the uncoupled atmospheric component, the uncoupled NCAR CSM Ocean Model (NCOM), and the fully coupled CSM (Kiehl et al., 1998) show that a major cause of the bias in the CSM model is the excess of shortwave radiation reaching the ocean surface. Since the dynamical efficiency of ocean heat transport is small where the SST is warm, the coupled system could respond by changing its gradient.

To better elucidate the ability of the model to reproduce the LGM SST in different regions of the Atlantic Ocean, the SST difference (LGM minus Present Day) is compared with three available data-based reconstructions. The first one is the BLGM data set (Trend-Staid and Prell, 2002). They apply the modern analog technique (MAT) to reconstruct SST at the LGM using a database of 292 planktonic foraminiferal samples located mostly in the Atlantic and Indian Oceans. The second one, the TEMPUS (Rosell-Melé, 1998) data-set, is based on alkenone sediment data from the Nordic seas and North Atlantic which are compared to those from Sikes et al. (1997) for the Southern Ocean to evaluate further U_{37} and U_{37}' as proxies to estimate cold temperatures. The last data-set is the Niebler et al. (2003) data-set. They use planktonic foraminiferal assemblages in 70 sediment cores from the tropical and subtropical South Atlantic Ocean (10°N–37°S) to estimate annual mean SST. In Fig. 4, the location and LGM − PD SST differences for each site are superimposed on the contours of the LGM − PD SST difference of the coupled model. To easily compare the different sites with the model, the region is divided into four boxes (west and east Equatorial and South Atlantic (SA)), delimited by the thin dashed lines on Fig. 4. The proxy data sets do not show good agreement with some nearby sites showing differences as much as 2–3 °C. The spatial distribution of the proxy data is denser in the equatorial box and in the eastern SA box. The greatest LGM cooling for proxy data and model relative to the PD is found in the eastern equatorial region and near the African coast.

The main feature of this region is the Benguela Current and the associated upwelling system. At 30°S, the entire Benguela Current is confined between the African coast and the Walvis Ridge near the Greenwich Meridian (Garzoli and Gordon, 1996). Bordering this current on its landward side is a coastal upwelling region that supports the local fisheries. The Benguela system is

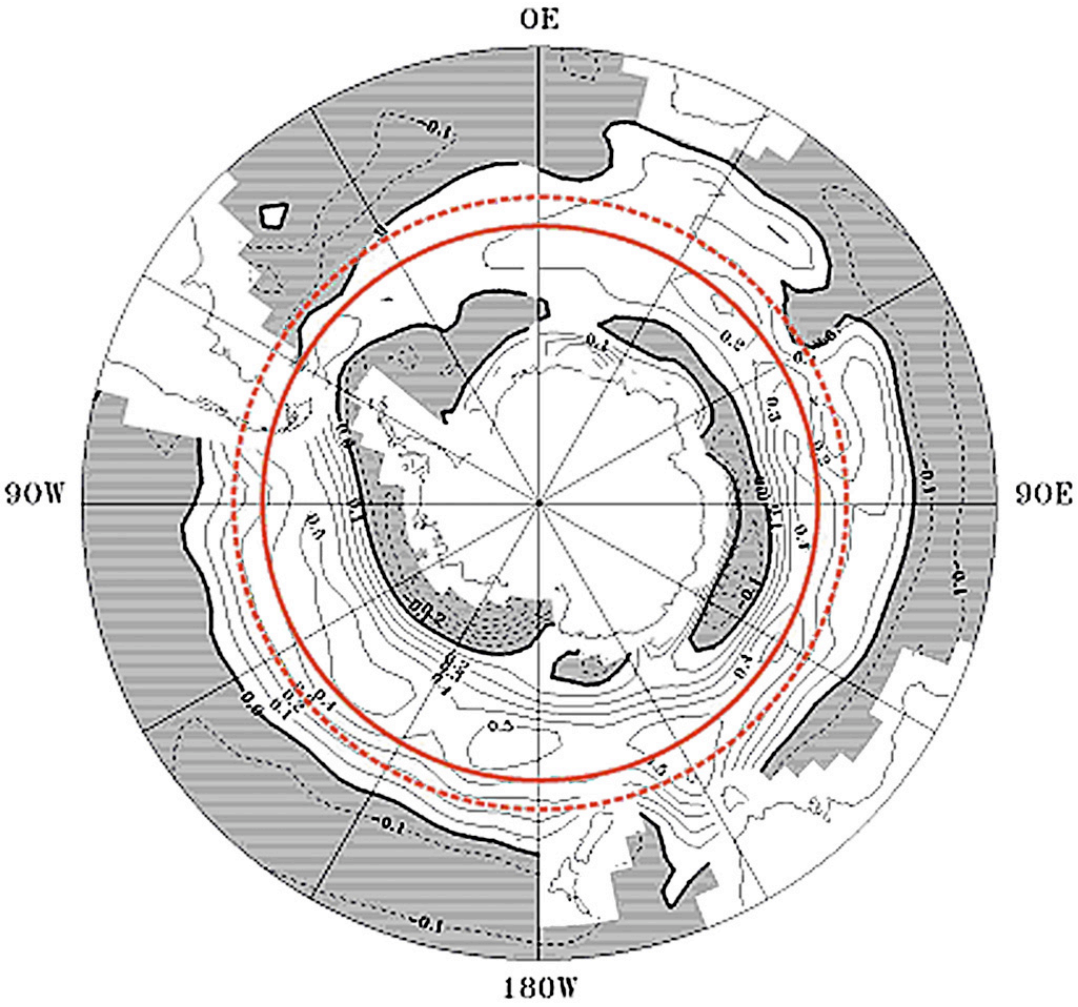

Fig. 8. The annual zonal wind stress (N m^{-2}) changes (LGM − PD). Positive values are shaded in lighter gray and negative values are in darker gray. The red lines show the position of the maximum averaged zonal wind stress (full line for the LGM and the dotted line for the Present Day). The contour interval is 0.1 N m^{-2}. (For interpretation of the references to colour in this figure legend, the reader is referred to the web version of this article.)

characterized by seasonal and interannual changes, mainly modulated by the winds. Off Namibia in the northern part of the Benguela system, there are seasonal changes with increased intensity of winds towards the Equator in winter, resulting in increased upwelling. These winds are calmer in summer, resulting in reduced upwelling and warmer surface waters. The CSM simulations are developed to represent global scale features. Local processes are not well represented due to lack of appropriate resolution. The cold tongue seen by the observations in the southeast Atlantic is one of these processes. The model fails to resolve the interaction between the deep ocean and the coastal shelf, which does not allow for the representation of the expected coastal upwelling in this region. Moreover, the winds in the model in the southeastern Atlantic are too weak contributing to the lack of realistic upwelling (due in part of the bias mentioned earlier).

The model LGM − PD SST differences are zonally averaged in each box and plotted with the available proxy data plotted as a function of the latitude of the site location (Fig. 5). The western SA region (Fig. 5a) has the fewest number of proxy-data sites and shows in average large SST differences with respect to the model. The two estimates from Niebler et al. (2003) in this region are in good agreement with the model average. In the eastern SA region (Fig. 5c), the average proxy SST difference appears to be in better agreement with the model, in particular, north of 35°S. Some sites of Niebler et al. (2003) show very anomalous values, around −6 °C. In the equatorial region, the west and east boxes show two distinct patterns. In the western box (Fig. 5b), the model predicts a zonal mean LGM cooling between 1 and 2 °C with slightly greater cooling toward the north. The BLGM data-set show slightly weaker LGM cooling. Both data-sets present some anomalous

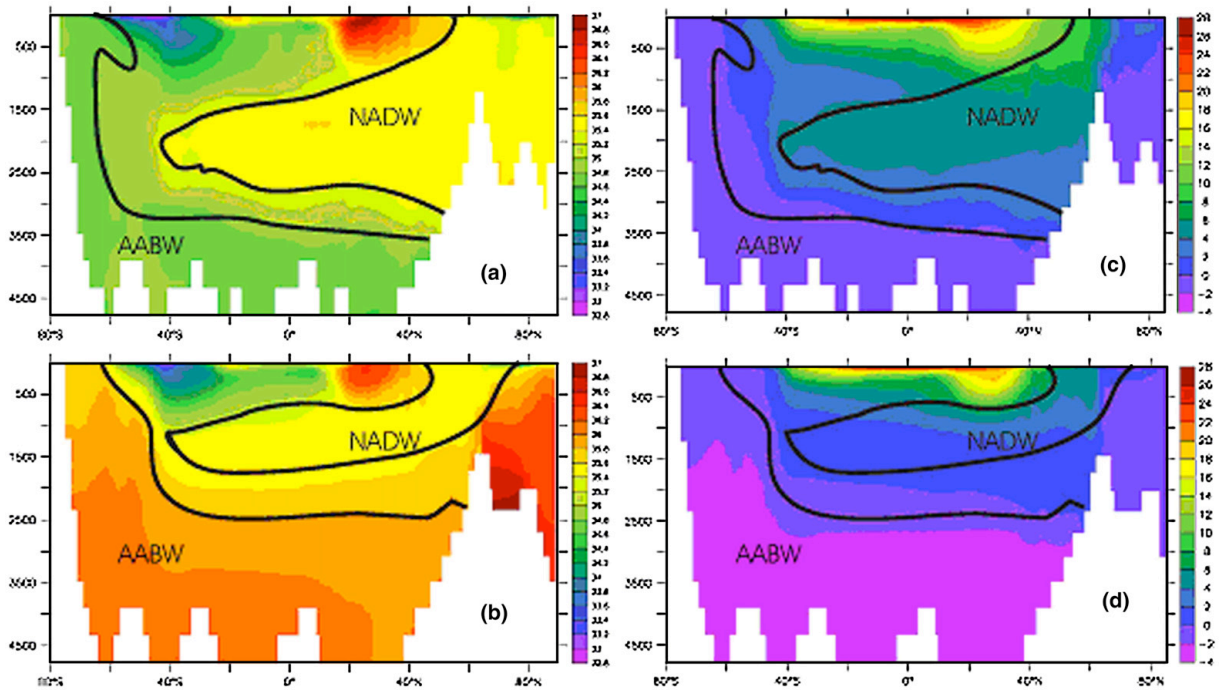

Fig. 9. The Atlantic Ocean cross section of the zonally averaged of salinity (psu) (left panels) and temperature (°C) (right panels). The black line delimits the Antarctic Bottom Water (AABW) and the North Atlantic Deep Water (NADW): (a)–(c) Present Day; (b)–(d) LGM.

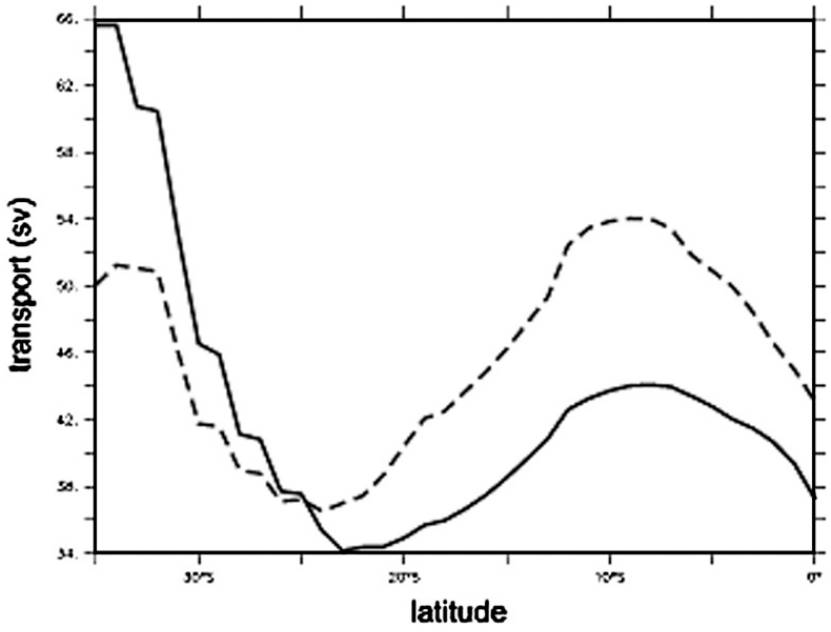

Fig. 10. The annual meridional integrated northward mass transport (Sv) in the South Atlantic Ocean: dotted line for the LGM and solid line for the Present Day.

values near the Equator. The LGM cooling estimated by the proxy data in the eastern equatorial box (Fig. 5d) shows the greatest bias compared to the model estimate of LGM cooling. All the proxy estimates show greater cooling than the model at LGM especially near the Equator. The TEMPUS data set shows the smallest

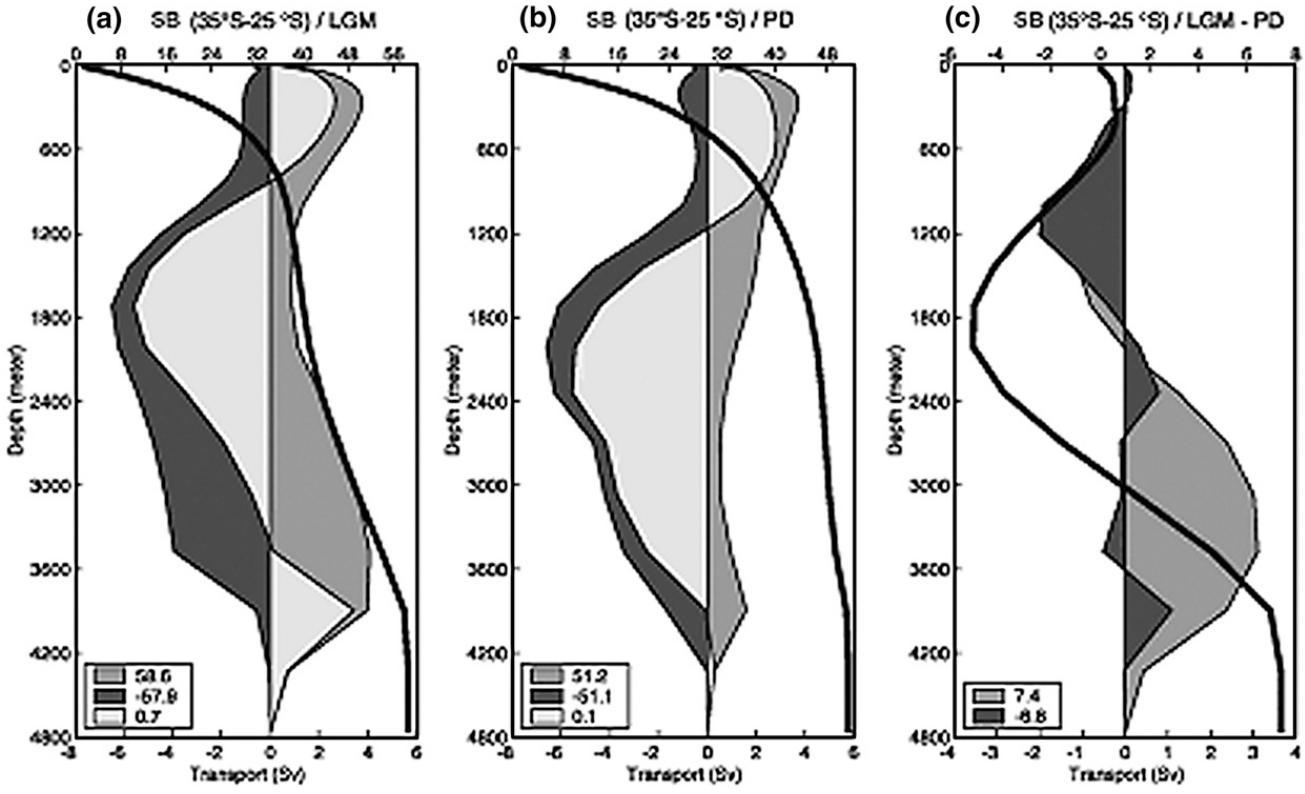

Fig. 11. Volume transport (Sv) in each layer averaged within the Southern Box (SB) (35°S to 25°S) for the Present Day, LGM and the difference (LGM − PD). Positive fluxes are to the north. The legend shows the total transport in each direction. In dark gray is the northward transport; black the southward and light gray the net transport (bottom *x*-axis). The thick black line shows the total northward-integrated transport (top *x*-axis).

latitudinal variation, with cooling estimated at about 3 °C. The two other data-sets show greater cooling at LGM of about −5 °C near the Equator.

3.3. Southern ocean transport

Taking into account that the Atlantic Ocean is an almost closed basin to the north, we first estimate the exchanges between the South Atlantic and other oceans for the two climatic periods. Fig. 6 shows the Pacific–South Atlantic Ocean mass exchange through the Drake Passage. The transports are divided into westward (black shading), eastward (grey shading) and net (light grey shading) flow for the LGM (Fig. 6a) and the PD (Fig. 6b). A significant increase of the eastward transport for the LGM (about 51 Sv) can be seen. The biggest difference in the mass transport between the two periods occurs at intermediate depths (approximately between 400 and 900 m), with a maximum value at 600 m (Fig. 6c). The thick black line shows the total integrated eastward transport. The difference shown in Fig. 6c between the integrated transports shows an almost linear increase between the surface and 1500 m. Below this depth the difference remains almost constant. The same intensification in the eastward mass transport is observed for the section between Cape of Good Hope and the Antarctic Peninsula (Fig. 7). The LGM transport is about 56 Sv larger than for the PD, mainly in the thermocline and intermediate layers, as in the Drake Passage case (Fig. 7c). The westward transport is also enhanced, showing an increase of the Agulhas leakage, predominantly in the deeper layers. The difference of the total integrated transport shows an increase between the surface and 1800 m with a maximum value close to 80 Sv. From this depth to the bottom, the difference remains almost constant.

The ACC intensification and associated increase in eastward transport (mainly in the intermediate layers for the LGM) can be explained primarily by the increase in the zonal wind (Fig. 8). The strengthening of the winds increases the northward Ekman transport, which reduces sea level in the southern part of the ACC and creates an anomalous northward pressure gradient. The direct consequence is an anomalous eastward geostrophic current in the same direction as the mean one, which acts to accelerate the ACC. A southward shift of approximately 3°, of the maximum zonal wind stress in the region (Fig. 8) goes hand in hand with the ACC intensification in the LGM. For example, Gent et al. (2001) discuss that the thermohaline circulation off the Antarctic shelf added to the Ekman transport is an important feature of the Drake Passage transport and consequently the ACC intensity. In this way, the enhancement of the Antarctic Bottom Water (AABW) production observed in the LGM simulation (Shin et al., 2003a,b) can also contribute towards the intensification of the ACC and its eastward transport.

Fig. 9 shows the meridional cross-section of the zonally averaged salinity (psu) for the Atlantic Ocean. The PD thermohaline indices of the water masses are those defined by Mamaev (1975). For the LGM, water mass indices are obtained from the averaged TS diagram of the Atlantic Ocean. The AABW is characterized by salinities lower than 34.8 psu and temperature lower than 2 °C for the PD. For the LGM, the salinities are lower than 36.6 psu and temperatures are lower than 1 °C. The limits of the NADW are defined by salinities ranging between 34.8 and 35.2 psu and temperatures between 3 and 4 °C for the PD. LGM values are salinities between 35.6 and 36 psu and temperatures between 1 and 2 °C. In other words, NADW and AABW are colder and saltier in the LGM. Whereas NADW is saltier than AABW in the PD, in the LGM AABW is saltier than NADW. The AABW becomes more salty at the LGM mainly due to the increase of the brine release associated with the formation of sea-ice. AABW forms under the regions of year-round sea-ice cover. The associated sea-ice melting and growth results in the vertically asymmetric redistribution of salt in the ocean, transporting more salt from the surface to the deep-ocean. These results are in agreement with the recent reconstruction by pore fluid measurements of the glacial salinity and temperature in sediment cores (Adkins et al., 2002). Adkins et al. (2002) proposed a reversal of the modern salinity contrast between the North and South Atlantic, where the saltiest water in the glacial deep ocean was found in the Southern Ocean. They suggest that this relative freshness in the region of the deep-water formation in the glacial North Atlantic can be consequence of a decrease in salt transport from the tropics by the Gulf Stream (Lynch-Stieglitz et al., 1999) coupled with tropical cooling (Stude et al., 1995) and associated decrease in evaporation. Boyle (2002), in highlighting the work of Adkins et al. (2002), shows an averaged salinity for the Atlantic deep waters of 34.9 psu and 36±0.2 psu for the present and LGM, respectively. These values are in very good agreement with the average of the model simulation: 34.85 and 36.18 psu for the PD and LGM simulations, respectively.

3.4. Meridional transport in the sub-tropics (Southern Box)

The integrated annual northward meridional mass transport in the South Atlantic is shown in Fig. 10. We can see two distinct patterns. The first one occurs in the

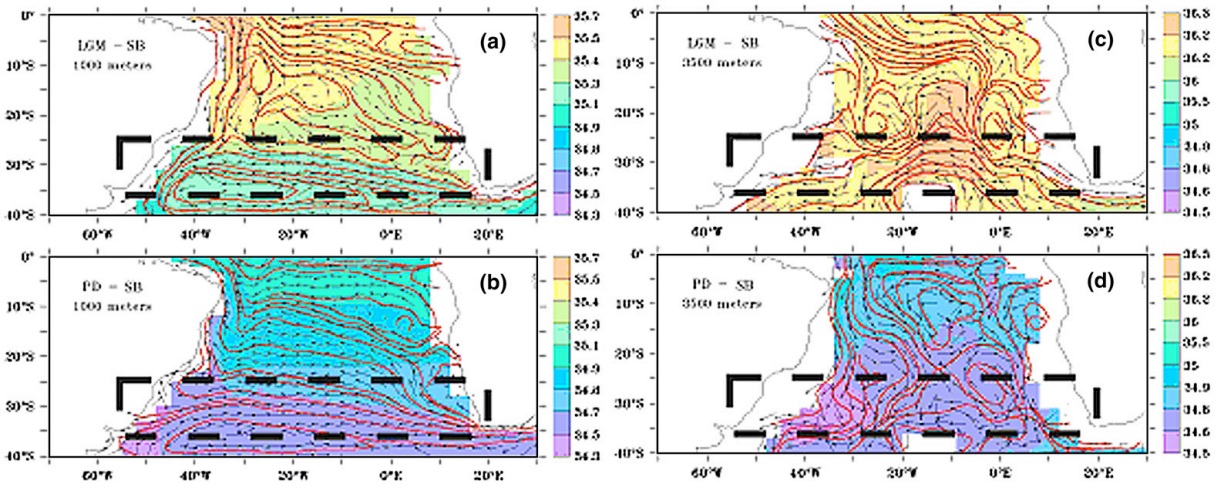

Fig. 12. Salinity (psu), horizontal current vectors (m s^{-1}) and streamlines (blue line) for the annual mean circulation for the Southern Box (SB) (region delimited by the dashed black box) along the depth of maximum difference in the mass transport between the Present Day (PD) and LGM: (a) LGM circulation at 1000 m; (b) PD circulation at 1000 m; (c) LGM circulation at 3500 m; (d) PD circulation at 3500 m. (For interpretation of the references to colour in this figure legend, the reader is referred to the web version of this article.)

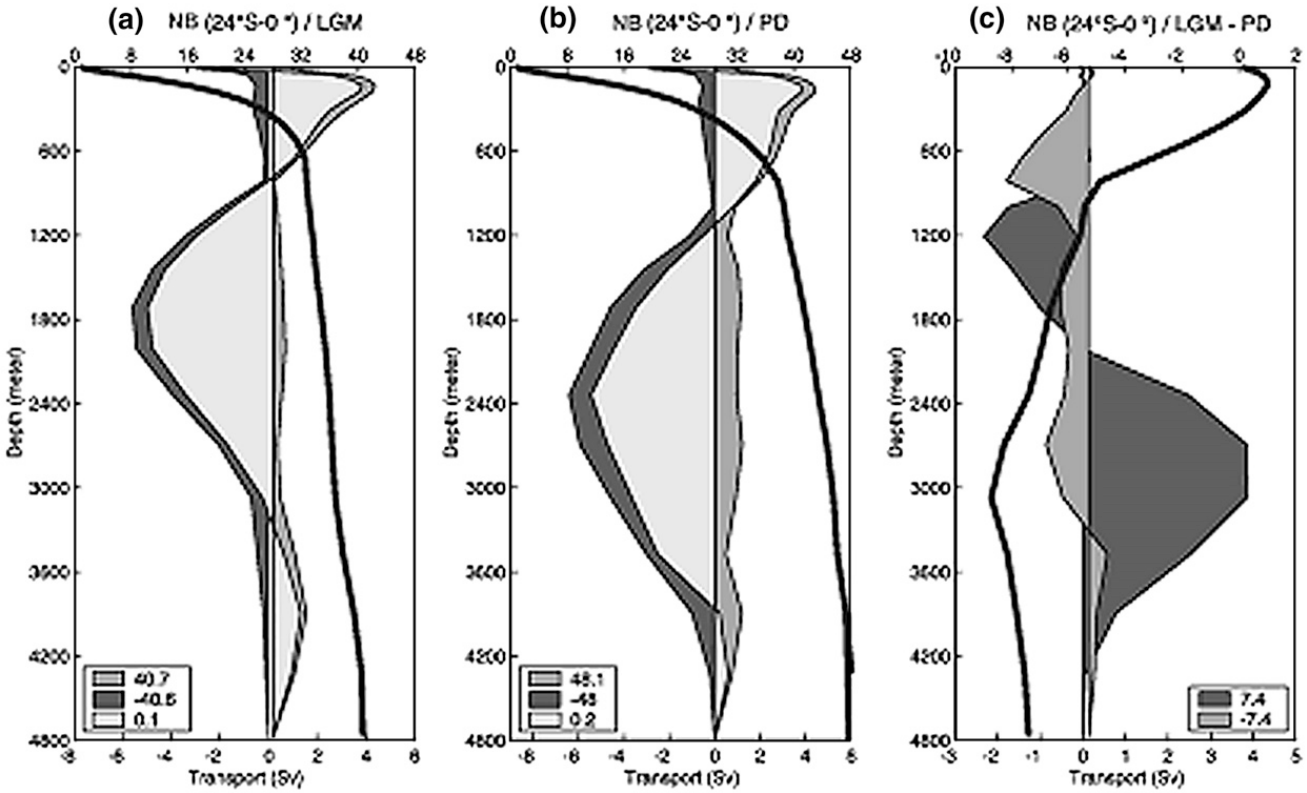

Fig. 13. Volume transport (Sv) in each layer averaged within the Northern Box (NB) (24°S to Equator) for the Present Day (PD), LGM and the difference (PD − LGM). Positive fluxes are to the north. The legends show the total transport in each direction. In dark gray is the northward transport; black the southward and light gray the net transport (bottom *x*-axis). The thick black line shows the total northward-integrated transport (top *x*-axis). (For interpretation of the references to colour in this figure legend, the reader is referred to the web version of this article.)

sub-tropics with an increase in the LGM transport (solid line) ranging from 25°S to 35°S, were the maximum difference with respect to the PD (dashed line) is 10 Sv. The second pattern shows a decrease in transport for the LGM between 25°S and the Equator, with a maximum difference between the two periods close to 12 Sv at 8°S. To examine in more detail these differences we calculate the average meridional transport between the two regions (referred now as Southern Box (SB – 35°S to 25°S) and Northern Box (NB – 25°S to Equator)).

The northward (dark grey shading), southward (black shading) and net (light grey) transport in the SB is depicted in Fig. 11. The zonal integral of the circulation consists of northward flow of the surface, thermocline and intermediate water, southward flow of the deep water and northward flow of the bottom water. This last one is more evident for the LGM. Comparing the two climatic periods yields that the net flow is about 7 Sv more intense at the LGM. For the northward flow, the biggest difference between the LGM and the PD (Fig. 11c) occurs in the deep layers (approximately 2700 to 3800 m), with a maximum of 3 Sv at 3500 m. For the southward flow, the biggest difference occurs in the intermediate layers (approximately 800 to 1500 m), with a maximum at 1000 m. The thick black line in Fig. 11 shows the total integrated northward transport. For the LGM (Fig. 11a) below 2000 m, the transport increases significantly (about 10 Sv).

For the PD (Fig. 11b), the total transport is almost constant (approximately 48–50 Sv) below 2000 m. This difference in the vertically integrated transport is clear in Fig. 11c and can be associated with the enhancement of the AABW intrusion into the SA (i.e. Fig. 9b). This increase is compensated by a decrease at intermediate depths which also suggests a weakening in the formation of the Antarctic Intermediate Water (AAIW).

In order to understand why the southward mass transport is larger for the LGM in the SB, we examine the circulation at given depths where the maximum difference between the two simulations is found. Fig. 12a,b shows the circulation at 1000 m for the LGM and the PD. The SB region is delimited by the thick dashed black box. The circulation is superimposed over the salinity at this depth in order to elucidate the effects of the different water masses. For the PD (Fig. 12b), the SEC reaches the Brazilian coast approximately at 25°S–30°S and splits into two. One branch flows to the north and the other flows southward feeding the BC. The salinity shows that

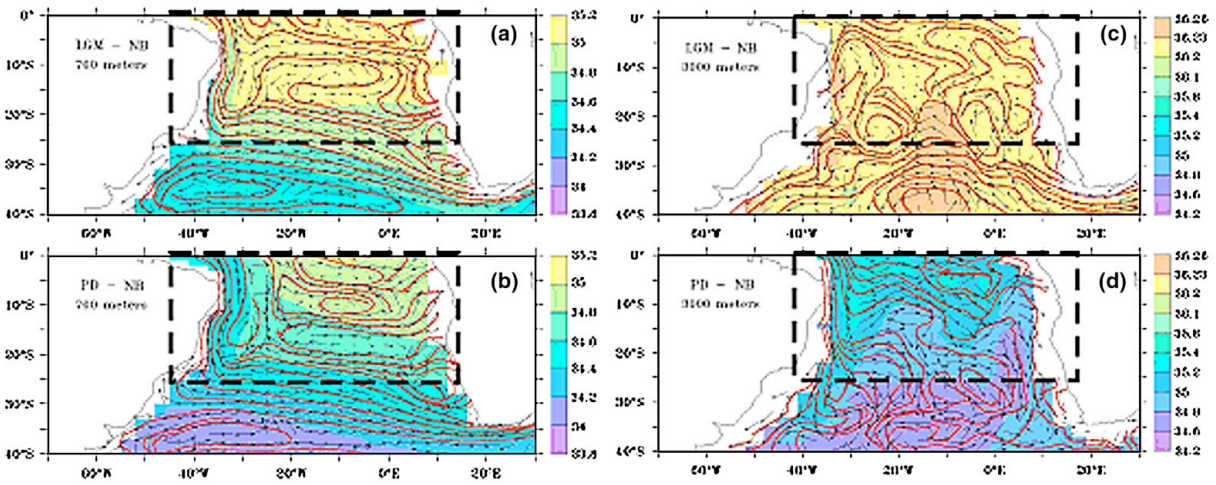

Fig. 14. Salinity (psu), horizontal current vectors (m s^{-1}) and streamlines (blue line) for the annual mean circulation for the Northern Box (NB) (region delimited by the dashed black box) along the depth of maximum difference in the mass transport between the Present Day (PD) and LGM: (a) LGM circulation at 700 m; (b) PD circulation at 700 m; (c) LGM circulation at 3000 m; (d) PD circulation at 3000 m.

the northward branch carries waters from the central part of the SA (around 34.7 to 34.9 psu) to the Equator, by the NBUC. For the LGM (Fig. 12a), the northern branch of the subtropical gyre also splits into two, however the southward flow is stronger and joins the strong western boundary current. The branch that flows north is not only weaker (with respect to the PD) but as it encounters the southward flow, a part of it deflects to the west and the other dissipates energy in two small gyres. High salinity water (over 35.4 psu) carried by the western boundary current spreads into the northern part of the SA. It blocks the SEC northward transport of the lower salinity water from the central part of the SA (observed at the PD). In other words, for the LGM SB region there is intensified southward flow that can be attributed to the strengthening of the BC and the associated BC recirculation cell.

The intensification of northward transport found in the deeper layers (3500 m) for the LGM can be seen in Fig. 12c. This intensification is due to the strong influx of Indian Water (IW) through the Agulhas leakage. The greater intrusion of the AABW into the South Atlantic (e.g. Fig. 12) contributes to the large northward transport. Salinity is homogeneous over the entire SA in the LGM, varying between 36.2 and 36.3 psu (i.e. Fig. 12). For the PD (Fig. 12d), the flow of the DWBC is the dominant circulation pattern. Its strong southward flow prevents the intrusion of the AABW and the inflow from the IW, consequently the intensification of northward transport, found for the LGM, is not present.

3.5. Meridional transport in the tropics (Northern Box)

As in the SB, the transport changes in the NB are in agreement with the zonally averaged water mass changes of the meridional section. Fig. 13 shows the northward (dark grey shading), southward (black shading) and net (light grey shading) transport at each model depth level for the NB. The net flow is southward in the thin Ekman layer of few tens of meters, then it reverses to a northward flow in the thermocline and intermediate depth range (approximately 40 to 800 m) (see Stramma and England, 1999; Lazar et al., 2002 for a description of the associated circulation), reverses again to a southward flow in the deeper layers and reverses again to the north in the bottom layers. The northward flow of thermocline waters is shallower in the LGM penetrating to 800 m compared to about 1000 m for PD. The southward flow is less intense at the deeper layers (between 2300 and 3500 m), with a maximum value of 4 Sv at 3000 m. A greater intrusion of the AABW can be seen in the enhanced northward transport in the deepest layers of the LGM. The total transport difference between the two simulations is approximately 7 Sv weaker for the LGM in both directions. The total integrated northward transport (thick black line) shows a similar pattern until 500 m between the two periods (Fig. 13a,b). From this depth to the bottom, the transport for the LGM is about 8 Sv weaker.

The meridional transport for the NB shows a weakening of the flow for the LGM in contrast to what was observed in the SB (intensification of the LGM flows). Fig. 14 shows the circulation at the depth of 700 m for the LGM (Fig. 14a) and the PD (Fig. 14b). The NB region is delimited by the thick dashed black box. There is a northward shift of the SEC bifurcation latitude, from 30°S (at the PD) to approximately 20°S–25°S (at the LGM) leading to a reduction of the northward flow. This shift also induces a weakening of the western recirculation of the central band of the SEC (CSEC). The CSEC flows southward at approximately 25°S, loops back northward, increasing the NBUC flow (in agreement with Stramma and England, 1999). This more intense northward flow in the PD transports lower salinity waters (around 34.4 to 34.6 psu) from the central part of the SA to the Northern Hemisphere. In the LGM, the higher salinity waters (around 35 to 35.2 psu) in the tropical region block the intrusion of fresh waters.

The deep circulation (3000 m) in the NB region is shown in Fig. 14c,d for the LGM and the PD, respectively. The enhanced southward flow for the PD is due to a stronger DWBC. Indeed, according to Stramma and England (1999), after the DWBC crosses the Equator, the NADW separates near the seamount chain at the northeastern tip of Brazil. The major part flows to the south and the rest flows eastward across the Atlantic towards the African coast. At the African coast, it shifts south flowing along the continent. In the LGM, the NADW flow is weaker and stays confined to the western boundary.

4. Conclusions

The analysis presented here provides an estimate of the coupled dynamical response of the South Atlantic Ocean to the LGM boundary conditions. The simulated SST is consistent with the proxy-data mainly in the South Atlantic region. The model overestimates the cooling in the southern SA (near 50°S) shown by the proxy-data. In the equatorial region, in spite of the scatter in the proxy estimations, the model appears to underestimate the cooling shown by all data sets in the eastern part of the basin. This can be explained by the known bias in the cloud representation in the model and consequently in the air–sea interaction dynamics, which tends to warm SST in

the eastern Atlantic for both periods (i.e. LGM and PD). The northward shift in the SCZ position suggests a compression and/or an equatorward shift of the subtropical gyre at the surface, consistent with what is observed in the proxy reconstruction (Trend-Staid and Prell, 2002; Pflaumann et al., 2003).

The enhancements of the ACC transport and consequently the exchange between the South Atlantic and the other oceans increases in part because of the intensification of the zonal wind stress at the LGM. The increase of the ACC transport is closely related to stronger Agulhas leakage. There is a poleward shift of the simulated zonal wind stress maximum, which contributes to a decrease in the blocking effect by the South America continent according to Klinck and Smith (1993), and consistent with Shin et al. (2003b) (Shin, 2002).

The zonal wind stress intensification in the LGM is confined to the Southern Ocean (i.e. Fig. 8) and does not have significant influence on the wind-driven circulation patterns ongoing the South Atlantic. However, in the intermediate and deeper layers the strong ACC transport contributes to an increase of the meridional mass transport in the LGM. The main changes observed in the mass transport, below the Ekman layer are consistent with the changes observed in the water mass formation. The increase of AABW formation at greater depth is compensated by the decrease in water mass formation at the intermediate depths. Likewise, thermocline waters' formation rate probably decreases since the upward shift of the NADW, which squeezes the thermocline, is not accompanied by the expected increase in the associated transport.

In the intermediate layers, an intensification in the southward mass transport in the SB region and a weakening in the northward mass transport in the NB for the LGM was observed. The SB intensification is due to the strengthening of the BC and the associated BC recirculation cell. Both of which are connected to the shallow Atlantic overturning circulation. With the intensification of the subtropical gyre, unequal branches of the SEC bifurcation occur. In the NB, the weakening of the northward flow in the LGM is due to a northward shift of the latitude of bifurcation of the SEC leading to a weakening of the northward flow and inducing a reduction of the western recirculation of the CSEC. The northward shift of the upper limit of the subtropical gyre (SEC) at intermediate depth added to the northward shift observed at the SCZ at the surface indicates a displacement of the subtropical gyre of 3°–5° latitude equatorward.

In the deeper layers, an intensification of the northward mass transport in the SB region and a weakening in the southward mass transport in the NS for the LGM is observed. A weaker and shallower NADW is associated with a greater intrusion of AABW. Besides the AABW intrusion, the increase of the IW inflow is also responsible for the SB northward intensification. In the NB, the weaker and shallow overturning circulation results in a weaker southward transport.

Acknowledgements

This work was supported in part by grants FAPESP-00/02958-7, FAPESP 01/04920-0, CNPq 300223/93-5 and CNPq 300040/94-6. IW also thanks the National Science Foundation for travel support to NCAR through the SGER programme.

Appendix A. List of acronyms

AABW	Antarctic Bottom Water
AC	Agulhas Current
ACC	Antarctic Circumpolar Current
BC	Brazil Current
BGC	Benguela Current
BMC	Brazil–Malvinas Confluence
CCSM3	Community Climate System Model Version 3
CLIMAP	Climate/Long Range Investigation Mappings and Predictions Project
CSEC	Central SEC Branch
CSM 1	Climate System Model Version 1
DWBC	Deep Western Boundary Current
EIC	Equatorial Intermediate Current
GLAMAP	Glacial Atlantic Ocean Mapping
ITCZ	Inter-Tropical Convergence Zone
IW	Indian Water
LGM	Last Glacial Maximum
MARGO	Multiproxy Approach for the Reconstruction of the Glacial Ocean Surface
MC	Malvinas Current
NADW	North Atlantic Deep Water
NB	Northern Box
NBUC	North Brazil Undercurrent
NICC	Northern Intermediate Countercurrent
NS	Northern Section
PD	Present Day
SA	South Atlantic
SAC	South Atlantic Current
SB	Southern Box
SCZ	Subtropical Convergence Zone
SEC	South Equatorial Current
SECC	South Equatorial Countercurrent
SS	Southern Section
SSEC	Southern SEC Branch

SSS Sea Surface Salinity
SST Sea Surface Temperature
WOA World Ocean Atlas

References

Adkins, J.F., McIntyre, K., Schrag, D.P., 2002. The salinity, temperature and $d^{18}O$ content of the glacial deep ocean. Science 298, 1769–1773.

Beal, L.M., Bryden, H.L., 1999. The velocity and vorticity structure of the Agulhas Current at 32°S. J. Geophys. Res. 104 (c3), 5151–5176.

Berger, A.L., 1978. Long-term variations of daily insolation and Quaternary climatic changes. J. Atmos. Sci. 35, 2362–2367.

Bonan, G.B., 1998. The land surface climatology of the NCAR land surface model (LSM1.0) coupled to the NCAR Community Climate Model (CCM3). J. Clim. 11, 1307–1326.

Boville, B.A., Gent, P.R., 1998. The NCAR Climate System Model, version one. J. Clim. 11, 1115–1130.

Boville, B.A., Hurrel, J., 1998. A comparison of the atmospheric circulations simulated by the CCM3 and CSM1. J. Clim. 11, 1327–1341.

Boyle, E.A., 2002. Oceanic salt switch. Science 298, 1724–1725.

Broecker, W.S., 1997. Thermohaline circulation, the Achilles heel of our climate system: will man-made CO_2 upset the current balance? Science 278, 1582–1588.

Broecker, W.S., Denton, G.H., 1990. What drives glacial cycles? Sci. Am. 262, 48–56.

Bryan, K., 1984. Accelerating the convergence to equilibrium of ocean–climate models. J. Phys. Oceanogr. 14, 666–673.

Bryden, H.L., Beal, L.M., 2001. Role of the Agulhas Current in Indian Ocean circulation and associated heat and freshwater fluxes. Deep-Sea Res. 48 (8), 1821–1845.

Clark, P.U., Mix, A.C., 2002. Ice sheets and sea level of the Last Glacial Maximum. Quat. Sci. Rev. 21, 1–7.

CLIMAP Project Members, 1981. The surface of ice-age earth. Science 191, 1131–1137.

Flato, G.M., Hibler, W.D., 1992. Modelling pack ice as a cavitating fluid. J. Phys. Oceanogr. 22, 626–651.

Fu, L.L., 1981. The general circulation and meridional heat transport of the subtropical South Atlantic determined by inverse methods. J. Phys. Oceanogr. 11, 1171–1193.

Garzoli, S.L., 1993. Geostrophic velocity and transport variability in the Brazil–Malvinas Confluence. Deep-Sea Res. 40, 1379–1403.

Gent, P.R., Bruan, F.O., Danabasoglu, G., Doney, S.C., Holland, W.R., Large, W.G., McWilliams, J.C., 1998. The NCAR Climate System Model global ocean component. J. Clim. 11, 1287–1306.

Gent, P.R., Large, W.G., Bryan, F.O., 2001. What sets the mean transport through Drake Passage. J. Geophys. Res. 106, 2693–2712.

Goni, G., Wainer, I., 2001. Investigation of the Brazil Current front variability from altimeter data. J. Geophys. Res. 106, 31117–31128.

Gordon, A., 1985. Indian–Atlantic transfer of thermocline water at the Agulhas Retroflection. Science 227, 1030–1033.

Gordon, A., 1986. Interocean exchange of thermohaline water. J. Geophys. Res. 91, 5037–5046.

Gordon, A., Greengrove, C.L., 1986. Geostrophic circulation of the Brazil–Falkland Confluence. Deep-Sea Res. 33, 573–585.

Hack, J.J., Kiehl, J.T., Hurrell, J., 1998. The hydrologic and thermodynamic structure of the NCAR CCM3. J. Clim. 11, 1179–1206.

Kiehl, J.T., Hack, J.J., Bonan, G., Boville, B.A., Williamson, D., Rasch, P., 1998. The National Center for Atmospheric Research Community Climate Model: CCM3. J. Clim. 11, 1131–1149.

Klinck, J.M., Smith, D.A., 1993. Effect of wind changes during the Last Glacial Maximum on the circulation in the southern Ocean. Paleoceanography 8, 427–433.

Knauss, J.A., 1996. Introduction to Physical Oceanography, 2nd edition. Prentice-Hall, pp. 152–156.

Large, W.G., Danabasoglu, G., 2006. Attribution and impacts of upper-ocean biases in CCSM3. J. Clim. 11, 2325–2334.

Lazar, A., Inui, T., Malanotte-Rizzoli, P., Busalacchi, A.J., Wang, L.P., Murtugudde, R., 2002. Seasonality of the ventilation of the tropical Atlantic thermocline in an ocean general circulation model. J. Geophys. Res. 107, 1–18.

Legeckis, R., Gordon, A., 1982. Satellite observations of the Brazil and Falkland Currents – 1975 to 1976 and 1978. Deep-Sea Res. 29, 375–401.

Levitus, S., Boyer, T.P., 1994. World Ocean Atlas 1994. Temperature, NOAA Atlas NESDIS 4, vol. 4. Natl. Oceanic and Atmos. Admin., Silver Spring, Md. 1129 pp.

Lynch-Stieglitz, J., Curry, W.B., Slowey, N.C., 1999. Weaker Gulf Stream in the Florida Straits during the last glacial maximum. Nature 402, 644–648.

Mamaev, O.I., 1975. Temperature–Salinity Analysis of World Ocean Waters. Elsevier Sci. Publishing. 374 pp.

Mix, A.C., 2003. Chilled out in the ice-age Atlantic. Nature 425, 32–33.

Mix, A.C., Bard, E., Schneider, R., 2001. Environmental processes of the ice age: land, oceans, glaciers (EPILOG). Quat. Sci. Rev. 20, 627–657.

Niebler, H.S., Mulitza, S., Donner, B., Arz, H., Patzold, J., Wefer, G., 2003. Sea-surface temperatures in the equatorial and south Atlantic Ocean during the Last Glacial Maximum (23–19 ka). Paleoceanography 18 (3), 902–914.

Norris, J.R., Weaver, C.P., 2001. Improved techniques for evaluating GCM cloudiness applied to the NCAR CCM3. J. Clim. 14, 2540–2550.

Otto-Bliesner, B.L., Brady, E.C., 2001. Tropical pacific variability in the NCAR Climate System Model. J. Clim. 14, 3587–3607.

Paul, A., Schafer-Neth, C., 2003. Modeling the water masses of the Atlantic Ocean at the Last Glacial Maximum. Paleoceanography 18 (3), 783–799.

Peltier, W.R., 1994. Ice age paleotopography. Science 265, 195–201.

Peterson, R.G., Stramma, L., 1991. Upper-level circulation in the South Atlantic Ocean. Prog. Oceanogr. 26, 1–73.

Pflaumann, U., Sarnthein, M., Chapman, M., Funnel, B., Huels, M., Kiefer, T., Maslin, M., Schulz, H., Swallow, J., van Kreveld, S., Vautravers, M., Vogelsang, E., Weinelt, M., 2003. The Glacial North Atlantic: sea-surface conditions reconstructed by GLAMAP-2000. Paleoceanography 18, 774–794.

Pickard, G.L., Emery, W.J., 1982. Descriptive Physical Oceanography – An Introduction, 4th ed. Pergamon Press, New York. 249 pp.

Pinot, S., Ramstein, G., Harrison, S.P., Prentice, I.C., Guiot, J., Stute, M., Joussaume, S., 1999. Tropical paleoclimates at the Last Glacial Maximum: Comparison of Paleoclimate Modeling Intercomparison Project (PMIP) simulations and paleodata. Clim. Dyn. 15, 857–874.

Quartly, G.D., Srokosz, M.A., 1993. Seasonal variations in the region of the Agulhas Retroflection: studies with Geosat and FRAM. J. Phys. Oceanogr. 23, 2107–2124.

Raynaud, D., Jouzel, J., Barnola, J.M., Chappellaz, J., Delmas, R.J., Lorius, C., 1993. The ice record of greenhouse gases. Science 259, 926–934.

Rintoul, S.R., 1991. South Atlantic interbasin exchange. J. Geophys. Res. 96, 2675–2692.

Rosell-Melé, A., 1998. Interhemispheric appraisal of the value of alkenone indices as temperature and salinity proxies in high-latitude locations. Paleoceanography 13, 694–703.

Sarnthein, M., Gersonde, R., Niebler, S., Pflaumann, U., Spielhagen, R., Thiede, J., Wefer, G., Weinelt, M., 2003. Overview of Glacial Atlantic Ocean Mapping (GLAMAP 2000). Paleoceanography 18 (2), 769–777.

Shin S.I., 2002. Understanding the climate of the Last Glacial Maximum using a climate system model. Ph.D. thesis at the University of Wisconsin-Madison, USA. 175 pp.

Shin, S.I., Liu, Z., Otto-Bliesner, B., Kutzbach, J.E., Vavrus, S.J., 2003a. Southern Ocean sea-ice control of the glacial North Atlantic thermohaline circulation. Geophys. Res. Lett. 30 (2), 68–71.

Shin, S.I., Liu, Z., Otto-Bliesner, B., Brady, E.C., Kutzbach, J.E., Harrison, S.P., 2003b. A simulation of the Last Glacial Maximum climate using the NCAR–CCSM. Clim. Dyn. 20, 127–151.

Sikes, E.L., Volkman, J.K., Robertson, L.G., Pichon, J.J., 1997. Alkenones and alkenes in surface waters and sediments of the Southern Ocean: Implications for paleotemperature estimation in polar regions. Geochim. Cosmochim. Acta 61, 1495–1505.

Stramma, L., 1989. The Brazil Current transport south of 23°S. Deep-Sea Res. 36, 639–646.

Stramma, L., England, M., 1999. On the water masses and mean circulation of the South Atlantic Ocean. J. Geophys. Res. 104, 20863–20883.

Stramma, L., Peterson, R.G., 1989. Geostrophic transport in the Benguela Current region. J. Phys. Oceanogr. 19, 1440–1448.

Stramma, L., Peterson, R.G., 1990. The South Atlantic current. J. Phys. Oceanogr. 20, 846–859.

Stude, M., Forster, M., Frischkorn, H., Serejo, A., Clark, J.F., Schlosser, P., Broecker, W.S., Bonani, G., 1995. Cooling of tropical Brazil (5 deg.C) during Last Glacial Maximum. Science 269, 379–383.

Sverdrup, H.U., Johnson, M.W., Fleming, R.H., 1942. The Oceans. Prentice Hall, Englewood Cliffs, NJ. 1087 pp.

Trend-Staid, M., Prell, W.L., 2002. Sea surface temperature at the Last Glacial Maximum: a reconstruction using the modern analog technique. Paleooceanography 17, 506–524.

Wainer, I., Gent, P., Goni, G., 2000. The annual cycle of the Brazil–Malvinas Confluence region in the NCAR Climate System Model. J. Geophys. Res. 11, 26167–26180.

Weatherly, J.W., Briegleb, B.P., Large, W.G., Maslanik, J.A., 1998. Sea ice and polar climate in the NCAR CSM. J. Clim. 11, 1472–1486.

Whitworth, T., Peterson, R.G., 1985. The volume transport of the Antarctic Circumpolar Current from the bottom pressure measurements. J. Phys. Oceanogr. 12, 960–971.